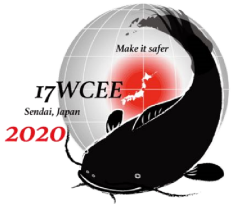

17th World Conference on Earthquake Engineering, 17WCEE
Sendai, Japan - September 13th to 18th 2020

TOWARD PHYSICS-BASED FAULT RUPTURE MODELS FOR SEISMIC HAZARD ASSESSMENT OF CRITICAL STRUCTURES

L. Dalguer[1], K. Yoshida[2], K. Irikura[3], K. Miyakoshi[4], Y. Matsumoto[5], T. Takahama[6],

[1] *Seismologist and Structural Engineer, 3Q-Lab GmbH, Switzerland, luis.dalguer@alumni.ethz.ch*
[2] *Researcher, Geo-Research Institute, Osaka, Japan, yoshida@geor.or.jp*
[3] *Professor, Aichi Institute of Technology, Toyota, Japan, irikura@geor.or.jp*
[4] *Researcher, Geo-Research Institute, Osaka, Japan, ken@geor.or.jp*
[5] *Researcher, Kozo Keikaku Engineering Inc., Tokyo, Japan, yasuhiro@kke.co.jp*
[6] *Researcher, Kozo Keikaku Engineering Inc., Tokyo, Japan, takahama@kke.co.jp*

Abstract

We have been investigating the phenomena of fault displacements and long-period ground motions near the surface rupture of past earthquakes for critical structures such as super high-rise buildings, long-span bridges, large oil tanks and nuclear installations. We are aware that for the evaluation and further understanding of such phenomena near the source, physics-based rupture models, as a complement of empirical approaches, may be appropriate, so that the predictions can be supported by physics, rather than purely empirical approaches. The main reason to use physics-based rupture models is that such phenomena are source-dominated phenomena, a feature that current empirical models are not capable to capture, mainly because of the sparseness of observed data near the source that posed challenges to provide meaningful and reliable ground motion and fault displacement predictions. This issue of lack of observed data is not only in magnitude and distance range, but also in frequency content range of ground motion as well as in site conditions such as on hard rock. The motivation to carry out this study is that the coseismic fault displacement and long period ground motion near the source associated to earthquakes may seriously compromise the safety of critical infra-structures and buildings located near faults. Therefore, this issue becomes critical for site-specific Seismic Hazard Analysis (SHA) and Fault Displacement Hazard Analysis (FDHA) of such critical infrastructures. Our final goal of this research is to bring the physics-based rupture models into practice of SHA and FDHA. For this purpose, simple and practical dynamic asperity fault models are used to evaluate past and future earthquake. The 2016 Mw 7.0 Kumamoto (Japan) earthquake is used as a case study to evaluate fault displacement and long period near-source ground motion. Surface-rupturing was observed along 34km of the main fault reaching values of fault displacement up to around 2.0m, as well as very near source ground motion has been recorded at stations with distance less than 1.0km from the surface rupture. The general procedure of dynamic rupture simulation follows the method proposed by Dalguer et al. (2019), in which the dynamic asperity models, as a first step, are constrained with kinematic asperity models already consistent with the observed near-source strong ground motion, and then the shallow layer (SL) zone of the fault is calibrated to predict fault displacement and long period ground motion at the very near-source. The main conclusions are as follow: 1) Two SL zones with enhanced energy absorption mechanism, respectively, in the NE and SW side of the fault are required to predict fault displacement consistent with observation. 2) In general, buried rupture penetrating the SL zone and surface rupture models can equally fit the observed ground motion and permanent displacement at the near-source stations. Implying that the surface rupturing contribution to the near-source ground motion is low, but the contribution of the SL zone is significant. 3) The surface rupture extension and fault displacement amplitudes are controlled by the shallow asperities, but the SL zone characteristics define the final fault displacement. 4) the ratio between the fault displacement and final slip at the SL zones is around 0.5. We argue that this ratio can serve as a metric to quantify the contribution of surface rupturing to the near source ground motion and permanent displacement.

Keywords: Physics-Based Fault Rupture Models, Asperity models, Strong Ground Motion Modeling, Fault Displacement Modeling, Seismic Hazard Analysis, Fault Displacement Hazard Analysis, Critical Structures.

1. Introduction

The reliable quantification of fault displacement caused by surface rupture and ground motion near the source have been recently of great concern for site-specific Seismic Hazard Analysis (SHA) and Fault Displacement Hazard Analysis (FDHA) for critical infrastructures such as super high-rise buildings, long-span bridges, nuclear power plants, nuclear waste depositories, chemical plants, dams, pipelines, etc., where studies are required to be done considering details of best available information of region-specific geology, site and seismic sources; as such, reliable non-ergodic models are needed that is contrary of current practice that uses empirical ergodic models based on global dataset that do not cover the whole range of interest. The development of empirical models to predict fault displacement and near-source ground motion for a site-specific region is up to date not feasible because the sparseness of observed data. This concern is reflected in the different efforts made by national and international agencies. For example, the International Atomic Energy Agency (IAEA) is making the effort to introduce the use of physics-based models for ground motion prediction [1, 2, 3, 4] as well as for fault displacement prediction [5], respectively for applications in Probabilistic Seismic Hazard Analysis (PSHA) and Probabilistic Fault Displacement Hazard Analysis (PFDHA) for nuclear installations.

Due to the insufficient of empirical models to address these issues reliably, there is a need to develop models, in which the predictions are meaningful from physics point of view. Therefore, the dynamic rupture models that take into account the physics of frictional sliding and wave propagation [e.g. 6, 7, 8, 9, 10] appear to be the best available approaches to address these issues. In addition, these physics-based models take into account the finite fault rupture, the geological and site conditions, making them as ideal models for fully non-ergodic studies because they are constrained with all the available information of the area of interest.

With the goal to address these issues we have been investigating the phenomena of fault displacements and long-period ground motions near the surface rupture of past earthquakes to develop simple and practical physics-based models for the assessment of future earthquakes. One output of this investigation is the model proposed by Dalguer et al. (2019)[11], in which we have proposed dynamic asperity models. In general, this approach consists of two steps. The first step is the characterization of asperities at the seismogenic zone based on the kinematic asperity source model, for example following Irikura's Recipe [12, 13] for strong ground motion prediction. In the second step, the shallow layer zone is characterized, so that the prediction of fault displacement, permanent displacement and the long period ground motion be consistent with the observations.

In this paper we use the method of Dalguer et al. (2019)[11] to investigate the fault displacements and long-period ground motions near the surface rupture of the 2016 Mw 7.0 Kumamoto (Japan) earthquake. This earthquake ruptured the earth surface along 34 km of the main fault, as reported by Shirahama et al. (2016)[14]. Strong ground motion of this event has been recorded by near-source stations from K-NET, KiK-net, and F-net operated by NIED [15, 16], and by stations from the JMA seismic intensity observation network [17]. This includes very near source ground motion stations at distance less than 1.0km from the surface rupture. Field investigation carried out by Shirahama et al. (2016) [14] on the day of the mainshock to map coseismic ruptures and measure their displacements indicates that surface ruptures appeared along the eastern part of the Futagawa fault zone and the northernmost part of the Hinagu fault zone, suggesting that this earthquake ruptured these two fault systems with fault displacement up to around 2.0m at Futagawa fault. Figure 1 shows the location of the surface rupture as well as the measurements of the fault displacements for horizontal (Figure 1a) and vertical (Figure 1b) components reported by [14]. The main objective of this paper is to develop dynamic asperity rupture models based in the kinematic asperity model developed following Irikura's Recipe [12, 13], so that the synthetic near-source ground motion, permanent displacement and fault displacement be consistent with observations.

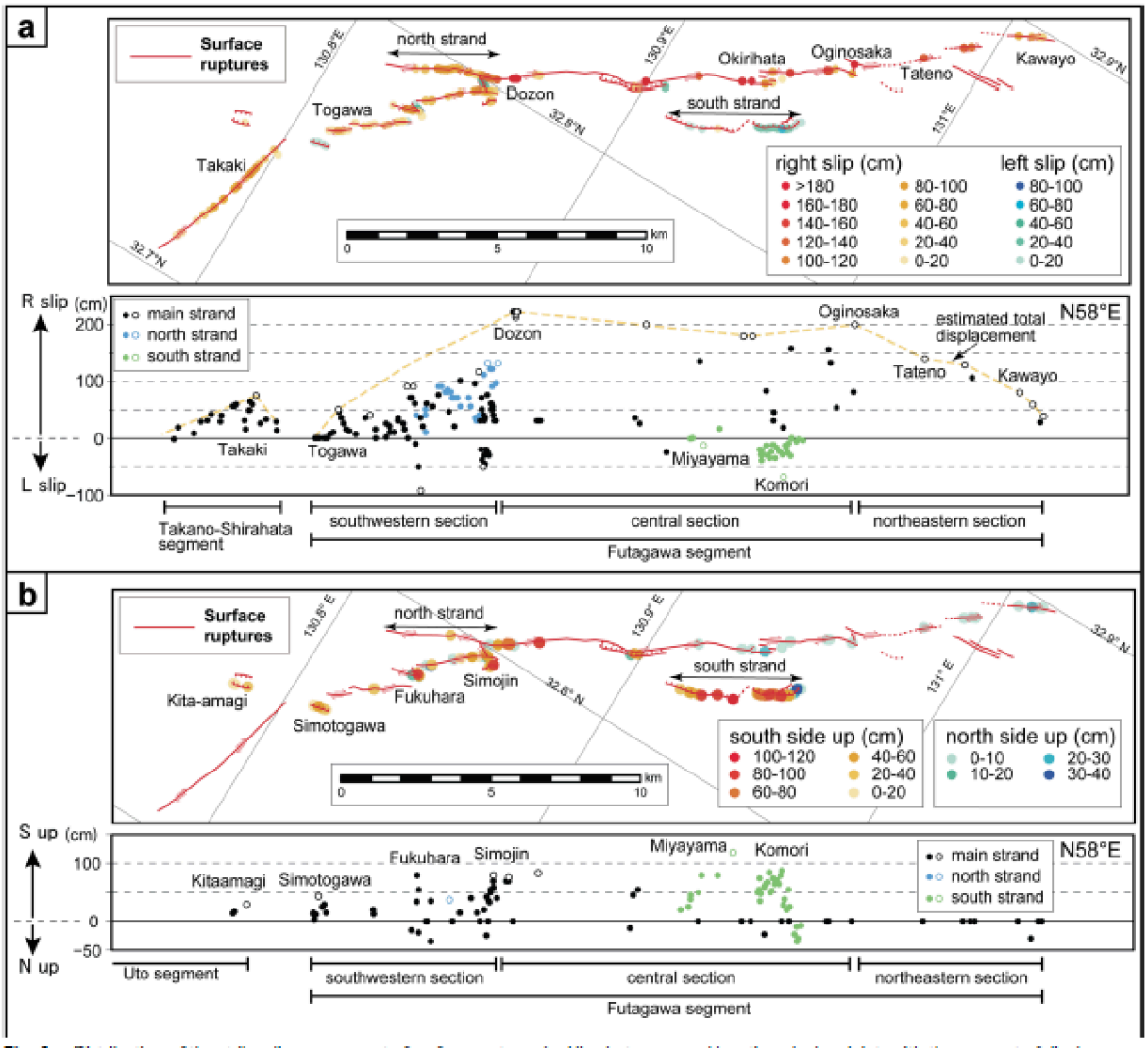

Fig. 1 – Detail fault trace map of surface rupture (red line) and measured fault displacement for horizontal (a) and vertical (b) component. Dashed yellow line at the bottom of (a) is the estimated total fault displacement (After Shirahama et al. 2016 [14]).

2. Dynamic rupture parameterization

We develop a simplified dynamic rupture model in a planar fault with dip angle of 65º, a strike angle of 236º and rake angle of 210º. Slip weakening friction in the form given by Andrews (1976) [6] is used as constitutive model for dynamic rupture simulation. The parameterization of the stress parameters is based on a kinematic asperity model developed Irikura's Recipe (Figure 2). As shown in Figure 2, the fault dimensions are assumed to have a length of 44km and a width of 19km. The kinematic fault model is composed of three asperities named as SMGA1, SMGA2 and SMGA 3, respectively with average slip 3.2m, 3.2m, and 4.2m. Where SMGA is the strong motion generation area at the seismogenic zone (Figure 2). In addition, the kinematic model also considers two patches of long period ground motion generation area (LMGA2 and LMGA3).

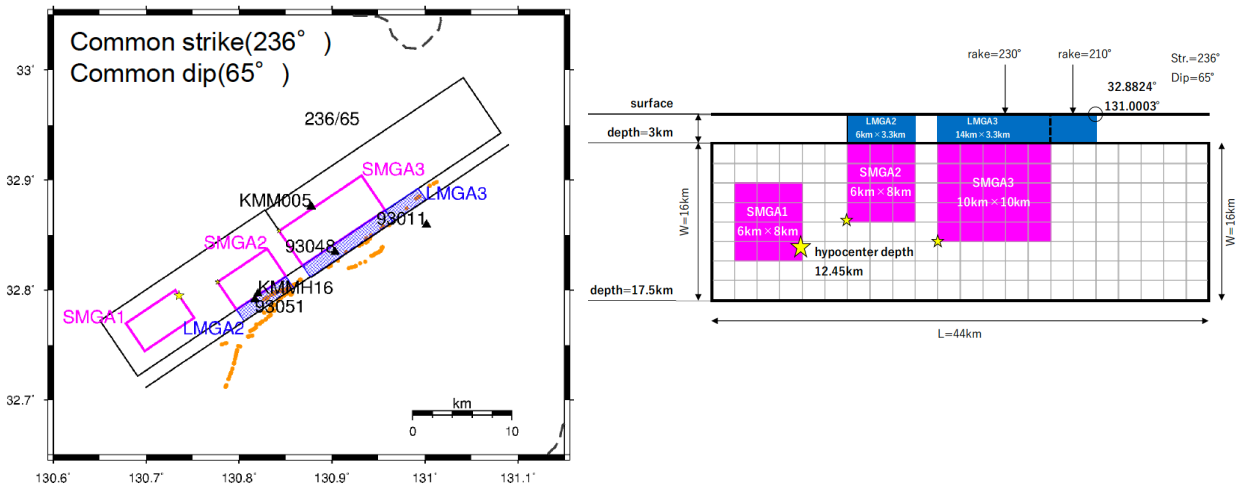

Fig. 2 – Kinematic asperity model developed following Irtikura's Recipe. (left) Map that shows the fault and stations location. (right) Asperity fault model

2.1 First step: Models without surface rupture

The first step of the dynamic rupture calculation is to find a model consistent with the kinematic asperity model without surface rupture. The initial stress drop distribution is computed given the distribution of static slip from the kinematic model. For this purpose, we use the approach from Andrews (1980)[18] and expanded by Ripperger and Mai (2004)[19]. This method follows the concept of a static stiffness function that involves a 2D-Fourier Transform of the slip on the fault. After calculating the initial stress drop distribution, a trial and error procedure is followed to estimate the stress drop at each asperity, so that the average slip at each asperity be approximately consistent with the ones from kinematic model. This initial calculation before starting the dynamic rupture simulations gives results of stress drops 13.0 MPa, 11.0 MPa and 12.0MPa, respectively for SMGA1, SMGA2 and SMGA3. In this first step a total of 10 models, denoted as MaspBs have been generated. Final stress drops of 17.3MPa, 7.0MPa and 10.9MPa, respectively for SMGA1, SMGA2 and SMGA3 have been obtained. The SL zone in this step is not calibrated, instead this zone is parameterized in order to inhibit surface rupture but allowed to penetrate the SL zone. So, the SL parameterization in all the B models have artificially large strength excess (SE). The Dc is depth dependent varying from 2m in the free-surface to a Dc of the seismogenic zone. At this point, Dc in the SL zone for the B models is just arbitrary, as a first trial for the second step. The final parameterization at the seismogenic zone obtained in this first step is shown in Table 1.

Table 1 – Final values of dynamic parameters at the seismogenic zone developed in the first step for models without surface rupture

	SMGA1	**SMGA2**	**SMGA3**	**Background of SMGA1**	**Background**	**Nucleation**
Dc (m)	0.4	0.4	0.4	0.4	0.4	0.4
Strength excess (MPa)	8.0	5.0	8.0	14.0	8.0	-0.87
Stress drop (MPa)	17.3	7.0	10.9	0.0	0.0	17.3

2.2 Second step: Models with surface rupture

In this second step, the SL zone parameterization is calibrated, while keeping the same dynamic parameterization at the seismogenic zone obtained in the step 1 (Table 1), so that surface rupture be approximately consistent with observed fault displacement reported by Shirahama et al. (2016)[14] shown in

Figure 1.The goal of this second step is to find an appropriate model that closely reproduce the observed fault displacement. For the calibration of the SL zone, it is first assumed that the dynamic parameters in this zone are homogeneous along strike and vary only with depth. Then a two SL zones along strike has been defined. In order to evaluate the influence of the asperities, the LMGA patches defined by the kinematic asperity model (Figure 2) are not used as constraints to define the SL zone.

Homogeneous SL zone (one SL zone)

A total of 12 models have been developed assuming a homogeneous SL zone along strike. We started varying the critical slip distance and strength excess with linear depth dependent and non-depth dependent while keeping a stress drop equal to zero. We found that larger critical slip distance (from 5m to 6m) are needed to produce reasonable fault displacement and slip amplitude in the SL zone. The preferred models with homogeneous SL assumption are MaspSS10 and MaspSS11. These two models equally predict the same near-source ground motion and permanent displacement, but main differences are in the fault displacement. Figure 3 shows the comparison of fault displacement for these two models with observations. The quantitative analysis of these two models is as follow: the misfit of maximum total fault displacement compared to the estimated value of Shirahama et al. (2016)[14] is 0.2m of MaspSS10 and 0.4m for MaspSS11; misfit of maximum horizontal fault displacement is =0.04m for MaspSS10 and 0.6m for MaspSS11; misfit of maximum vertical fault displacement is 0.19m for MaspSS10 and 0.08m for MaspSS11; extension (length) of surface rupture is better reproduced by MaspSS10 model. From this quantitative analysis, MaspSS10 is the best model assuming homogeneous SL zone. Table 2 shows the dynamic parameters for these two models. Notice that the only difference between these two models is the strength excess in the free surface, 1.2MPa for MaspSS10 and 1.5MPa for MaspSS11. These small differences in strength excess produce large differences in the final fault displacement, suggesting that small changes in the strength are very sensitive to the extension and amplitude of fault displacement. As shown in Figure 3, the models generate surface rupture extension and fault displacement amplitudes inconsistent with the observations at the NE site of the fault. This issue is expected to be addressed assuming a second SL zone in the NE site of the fault.

Table 2 – Dynamic parameters in the SL zone of best two models assuming homogeneous SL zone.

Model	MaspSS10		MaspSS11	
	Free-surface	Deep SL zone	Free-surface	Deep SL zone
Dc (m)	6.0	5.0	6.0	5.0
Strength excess (MPa)	1.2	4.0	1.5	4.0
Stress drop (MPa)	0.0	0.0	0.0	0.0

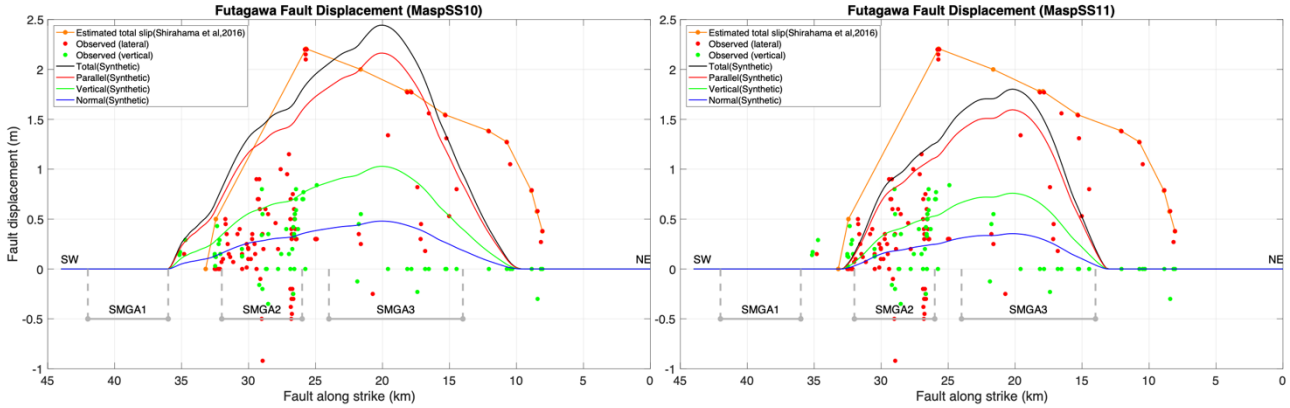

Fig. 3 –Fault displacement along the Futagawa fault compared with observations for models MaspSS10 (left) and MaspSS11 (right). The SMGA segments are projections of the three asperities. NE and SW show, respectively, the north-east and south-west of the fault.

Two SL zones

As shown in Figure 3, the assumption of homogeneous SL zone generates surface rupture extension and fault displacement amplitudes inconsistent with the observations at the NE segment of the fault. In order to produce further surface rupture at the NE, the goal is to add a second SL zone at the NE segment with little alterations to the surface rupture generated with the homogeneous SL. For this purpose, we change the strength excess to lower values at the NE, keeping the other dynamic parameters the same. We tested with values of 1.0MPa at the free-surface and 2.0 MPa at the deep of the SL zone in the two best models MaspSS10 and MaspS11 of the homogeneous case. The new models are now named, respectively MaspSS10S1 and MaspS11S1. The fitting to the observed fault displacement is significantly improved as shown in Figure 4. This figure shows the comparison of fault displacement from the two new models with observations. The quantitative analysis of these two models is as follow: the misfit of maximum total fault displacement compared to the estimated value of Shirahama et al. (2016) [14] is 0.25m of MaspSS10S1 and 0.39m for MaspSS11S1; misfit of maximum horizontal fault displacement is =0.02m for MaspSS10S1 and 0.59m for MaspSS11S1; misfit of maximum vertical fault displacement is 0.2m for MaspSS10S1 and 0.07m for MaspSS11S1; extension (length) of surface rupture is better reproduced by MaspSS10 model covering all extension from Shirahama et al (2016)[14] estimates and observed vertical component. The amplitude along the estimated values from Shirahama's is better reproduced by SS10S1 model along almost all the observed surface rupture length. From this quantitative analysis, MaspSS10S1 is the best model assuming two SL zones.

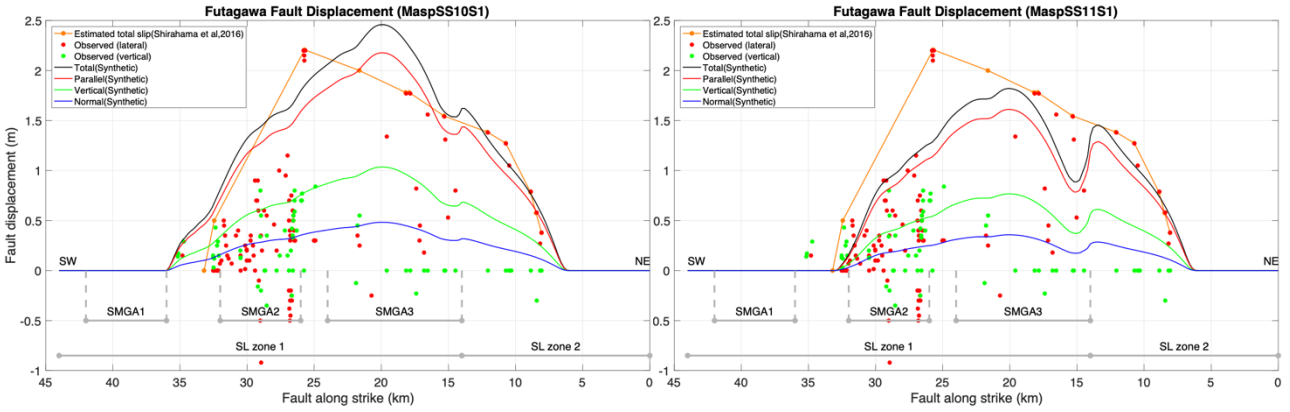

Fig. 4 – Fault displacement along the Futagawa fault compared with observations for models MaspSS10S1 (left) and MaspSS11S1 (right). The SMGA segments are projections of the three asperities. NE and SW show, respectively, the north-east and south-west of the fault. The two SL zones are also segmented at the bottom of the figure.

3. Dynamic rupture solution of best rupture models

The second step of the dynamic calibration of surface rupturing models discussed above has produced two best models, respectively, assuming homogeneous SL zone (model MaspSS10) and another assuming two SL zones (model MaspSS10S1). Figure 5 shows the dynamic input parameters, stress drop, strength excess and critical slip distance for these two models. The only difference between these two models is the strength excess at the SL zone. The rest of the parameters are identical. Figure 6 shows the dynamic rupture solution of these two models represented by the final slip, rupture time and rupture speed. As expected, no significant differences between these two models in all the solutions, except in the surface rupture and fault displacement shown in Figures 3 and 4.

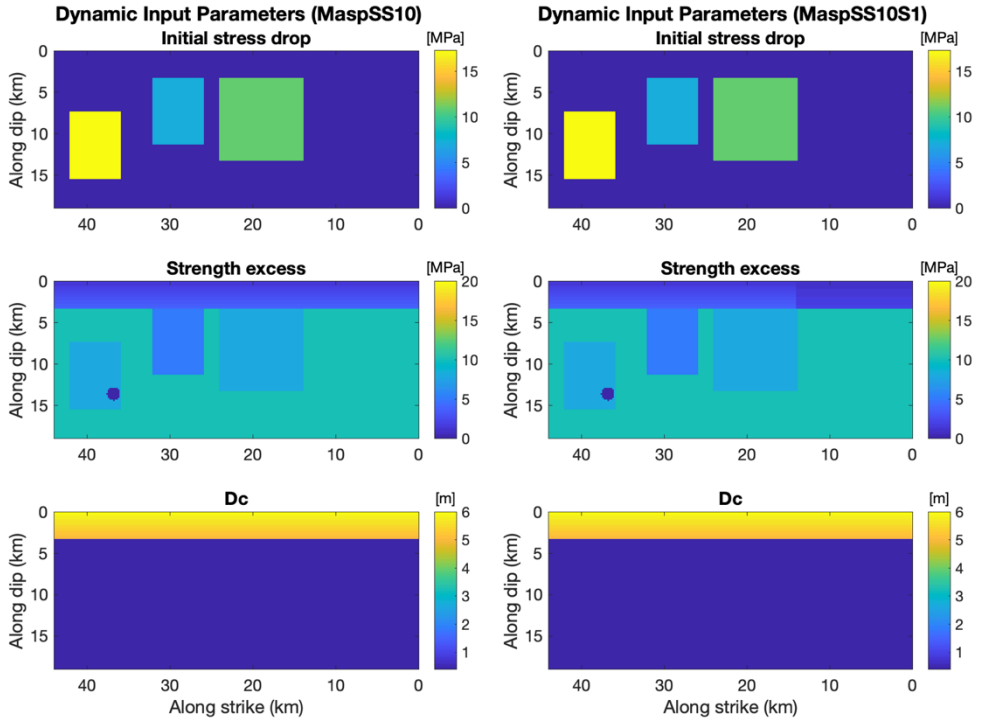

Fig. 5 –Dynamic stress parameters for dynamic rupture simulation of two best asperity models respectively for (left) homogeneous SL zone (model MaspSS10) and (right) for two SL zones (model MaspSS10S1). From top to bottom stress drop, strength excess and critical slip distance.

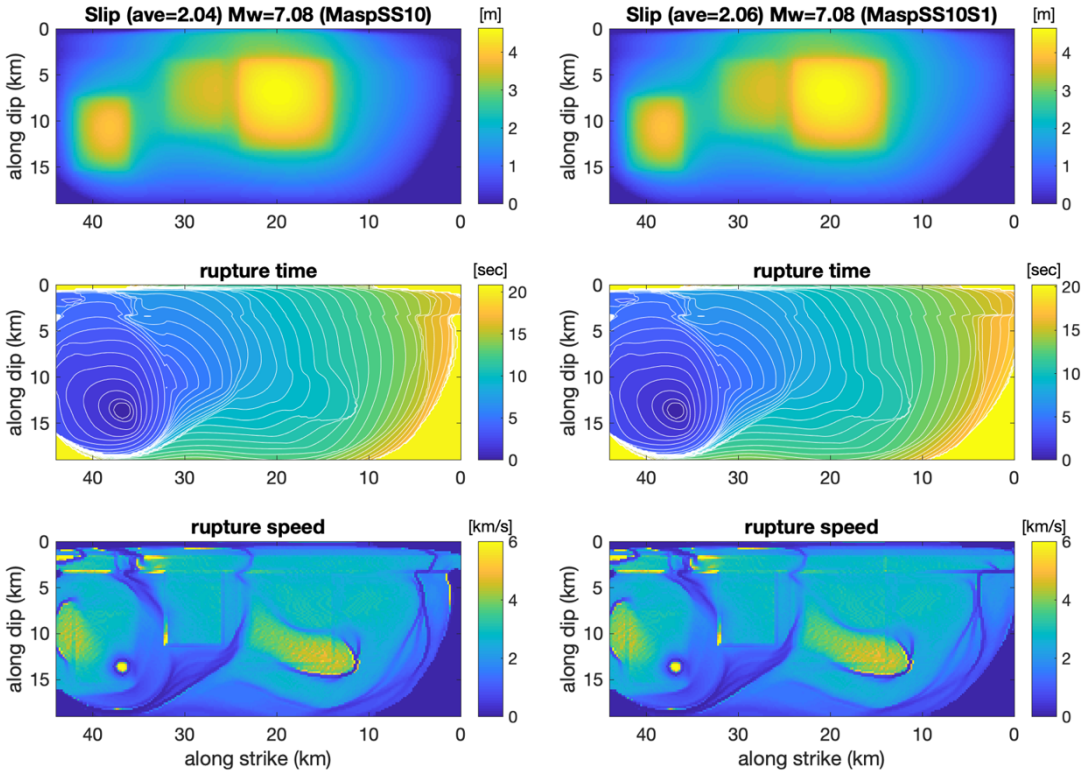

Fig. 6 –Dynamic rupture solutions of two best asperity models respectively for (left) homogeneous SL zone (model MaspSS10) and (right) for two SL zones (model MaspSS10S1). From top to bottom by the final slip, rupture time and rupture speed.

4. Near-source ground motion

In terms of near-source ground motion and permanent displacement at the observed stations, all the models, including the buried ruptures that penetrates the SL zone predict similar ground motion and permanent displacement as shown in Figure 7, where one buried rupture (MaspB6) that penetrates the SL zone is compared with the two best models with surface rupture respectively for homogeneous SL zone (model MaspSS10) and two SL zones (model MaspSS10S1). These results suggest that the surface rupturing contribution to the near-source ground motion is low, but the contribution of the SL zone is significant.

The ground motion generated by the two best models, are almost identical as seen in Figure 7. Overall, the very near source ground motions are consistent with the observations. But we can see some slight overestimation of the permanent displacement in most of the stations. The vertical component at station 93048 is underestimated. The reason of this underestimation may be due to different rake angle localized in the region of this station as shown by kinematic source inversions [e.g. 20]. As discussed in the first step section of buried rupture, models penetrating the SL zone without surface-rupture are good enough to reproduce the near-source ground motion and permanent displacement. Therefore, the major contribution to the permanent displacement at the near-source station comes mainly from the final slip at the SL zone. The fault displacement contribution with amplitudes consistent with observations is minor. This conclusion can also be implied from Figure 8 where slip profile with depth is shown. Slip at the SL zone is larger than the fault displacement, around double if we see the average slip. So, the ratio between fault displacement and slip at the SL zone is around 0.5.

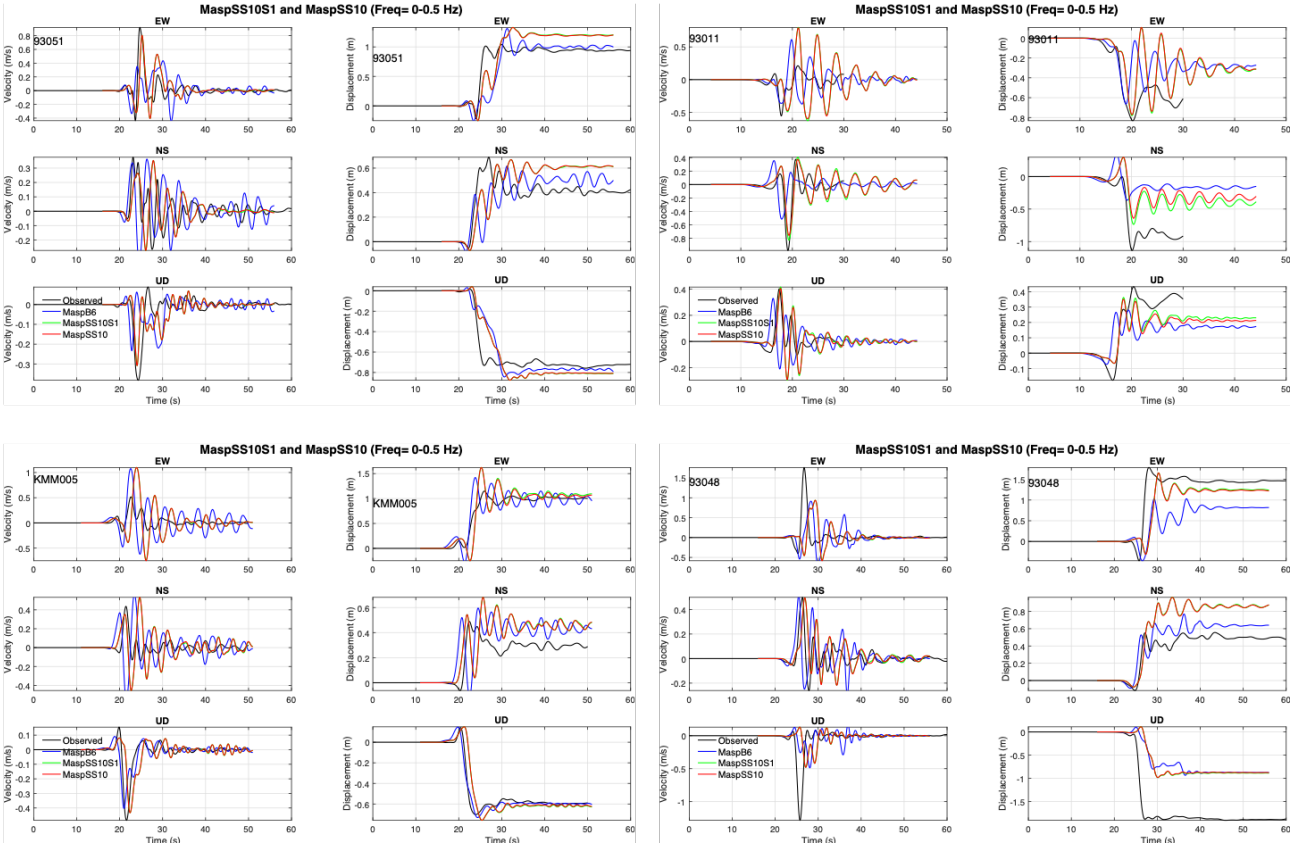

Fig. 7 –Three components of velocity and displacement ground motion from the two best models, respectively for homogeneous SL zone (model MaspSS10) and two SL zones (model MaspSS10S1) and a buried rupture that penetrates the SL zone, compared with four observed records at very near source stations.

5. Discussion and conclusions

5.1 SL zone and seismogenic zone

The general expectation that the SL zone contributes mainly to the long period ground motion and permanent displacement at the very near-source, and the SMGAs (asperities at the seismogenic zone) contributes to the high frequency ground motion is confirmed by the dynamic rupture simulations done in this study. The slip velocity functions of the best model (MaspSS10S1) at different points on the fault shown in Figure 8 corroborate this expectation. The slip velocity function at the SL zone is clearly dominated by smooth functions characteristics of long period generation. While the slip velocity functions at the seismogenic zone, in particular at the SMGAs and surroundings, is characterized by sharp function characteristics of high frequency generation.

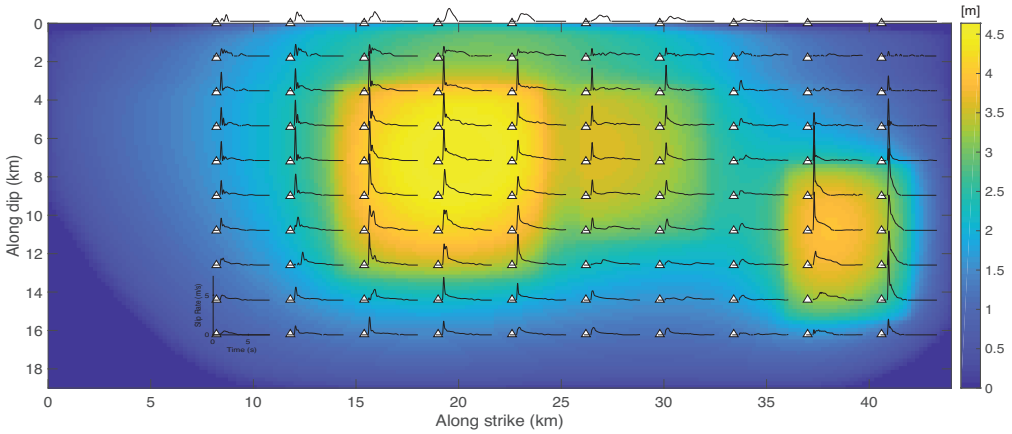

Fig. 8 –Slip velocity functions distributed at some points on the fault from the best model MaspSS10S1. Background correspond to the final slip distribution from the same model.

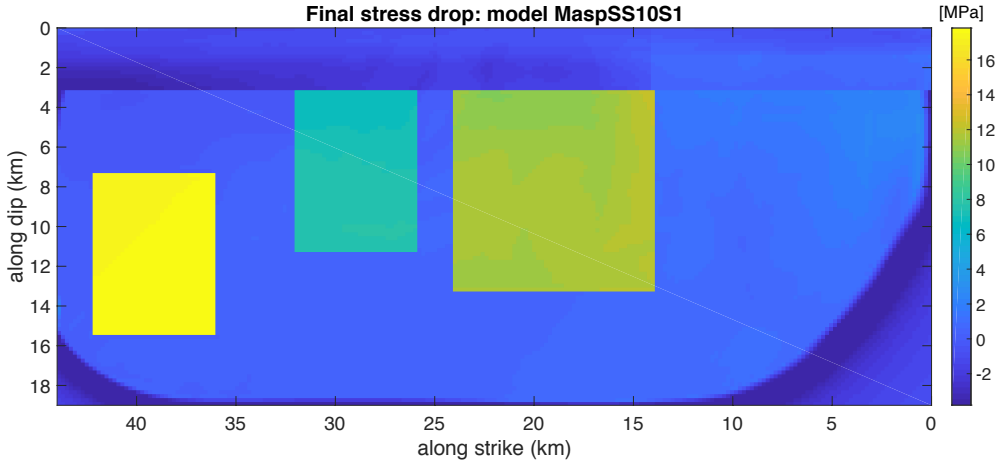

Fig. 9 –Final static stress drop distribution for the preferred model MaspSS10S1. Notice the dominated negative stress drop in the SL zone.

In the current study, we found large critical slip distance (Dc) (larger than 5m) for the SL zone in the preferred model (MaspSS10S1). When assuming zero nominal stress drop, this large Dc implies large energy absorption mechanism that results in negative stress drop. As seen in Figure 6, the final slip in the SL zone is lower than the Dc. It implies that the shear stress after reaching the yielding condition does not completely drop to the dynamic friction. The final shear stress (after the dynamic effect finish) accommodates to reach the static equilibrium resulting in a final static stress drop. Figure 9 shows the final static stress drop of the preferred model (MaspSS10S1). As shown in this figure, in the SL zone negative static stress drop is dominated due to the large Dc.

5.2 Surface rupture and fault displacement

The expectation of long period and short period generation area, as discussed in the previous section, is confirmed by this study. However, the contribution to the long period ground motion of surface rupture generating fault displacement seems to have very local effect in this study. The simulations done in the first step section of buried rupture shows that models penetrating the SL zone can equally predict the very near-source ground motion and permanent displacement (Figure 7). This suggest that the slip generated in the SL zone without surface rupturing can reproduce the observed long period ground motion and permanent displacement. This conclusion is corroborated by the simulations done in the second step where models with surface rupturing are generated. Almost all the surface rupturing models generate similar near-source ground motion and permanent displacement at the very near-source stations (Figure 7). The only differences between these models is the SL zone parameterization of strength excess and critical slip distance and the final results of fault displacement. Figure 10 shows the final fault displacement of all the surface rupturing models compared to the observed ones. Even though all the models generate similar ground motion and permanent displacement, the differences between them on surface rupture extension and permanent displacement amplitudes are large. Figure 11 shows depth profiles of dynamic parameters and along strike average slip of all the surface rupturing models and some buried rupture. Notice the major differences in the slip between the surface rupturing models is increasing gradually at the SL zone. This local effect of the surface rupturing is also corroborated by the introduction of two SL zones models. The second SL zone practically did not affect at all the very near-source ground motion and permanent displacement (see Figure 7). This second SL zone is needed to just locally fit the fault displacement at the NE site of the fault.

Further investigation is needed to understand why the surface rupturing effect is very local and the contribution is little to the near-source ground motion and permanent displacement. But on the basis of this study, one reason could be the large energy absorption mechanism that results in lower ratios between the fault displacement and final slip at the SL zone. In the simulations, as shown in Figure 10, this ratio seems to be in average 0.5. This ratio could be a metric to quantify the contribution of surface rupturing to the near source ground motion and permanent displacement. For a ratio of zero of course would be no contribution, then the increasing of this ratio will increase the contribution. The very first and rough criterium to define considerable contribution of surface rupturing would be when this ratio is larger or equal to 1.

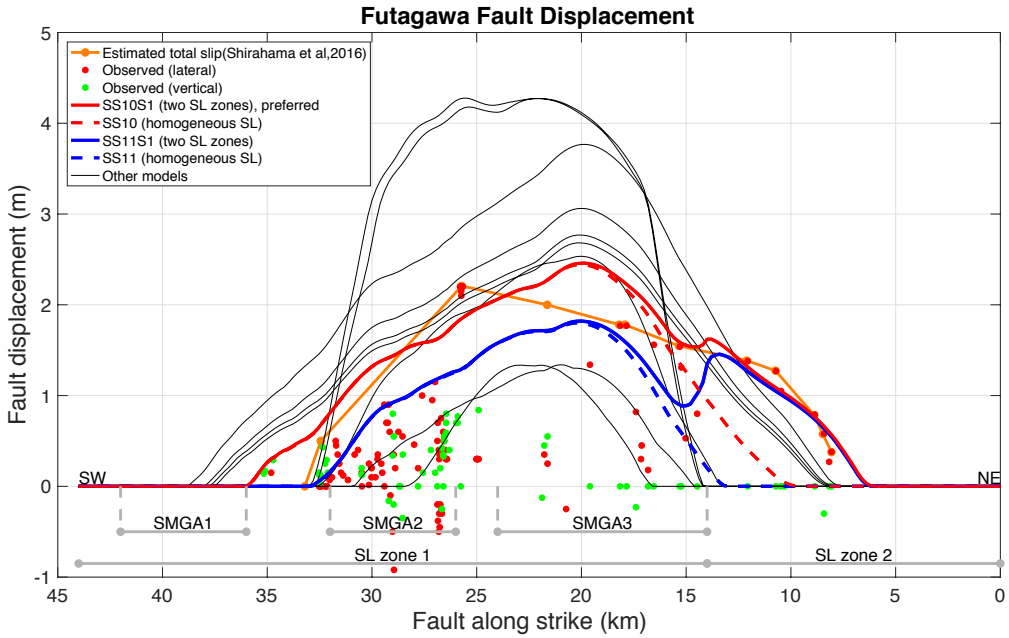

Fig. 10 –Fault displacement along the Futagawa fault compared with observations for all the surface-rupturing models. The SMGA segments are projections of the three asperities. NE and SW show, respectively, the north-east and south-west of the fault. The two SL zones are also segmented at the bottom of the figure.

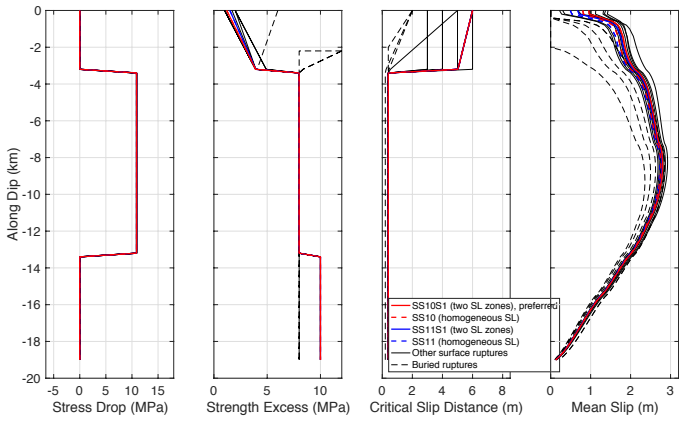

Fig. 11 –Dynamic parameterization profile (stress drop, strength excess and critical slip distance) along dip crossing the center of the asperity SMGA3 (19 km from the NE of the fault, see Figure 2) for all the surface rupturing models and some buried rupture (dashed black line). Right side of this figures shows the along strike average final slip with depth of all the models.

5.3 Asperity location, surface rupturing and LMGA

The shallow asperities are the main driving element of damaging earthquakes and also the one that promotes surface rupturing. This is because the major accumulation of energy is in the asperities. As seen in this study, surface rupturing is extended mainly above the shallow asperity. The extension and amplitude of the fault displacement would depend on the size and energy (stress drop) of the asperity, and of course on how deep is located the asperity. For example, in the current study, the amplitude of the fault displacement is larger above the SMGA3 asperity, as shown in Figures 3, 4 and 10. SMGA3 is the larger asperity in our asperity model. Overall, extension of the surface rupture will depend on three aspects, 1) how weak is the SL zone, 2) how strong is the SMGA to penetrate the SL zone and to break the free-surface, and 3) the depth location of the SMGA. For practical application of kinematic models, one need to define the long motion generation area (LMGA). Based on this study, two types of LMGA located in the SL zone can be defined, one with surface-rupturing and another without surface-rupturing. For practical issues, the depth location of the SMGA can be a key parameter to define criteria to set the two typed of LMGA. The surface rupturing effect can be defined with the expected ratio of fault displacement and slip in the SL zone. For ratios larger than around 1 the LMGA can be defined with surface rupturing.

6. Acknowledgements

This study is a part of the 2019 research project on fault displacement hazard assessment funded by the Secretariat of Nuclear Regulation Authority (NRA), Japan.

7. Copyrights

8. References

[1] IAEA. (2010). Seismic hazards in site evaluation for nuclear installations. *International Atomic Energy Agency— IAEA Safety Standards Series No. SSG–9*, Vienna (2010).

[2] IAEA. (2015). Ground motion simulation based on fault rupture modelling for seismic hazard assessment in site evaluation for nuclear installations. *International Atomic Energy Agency— IAEA Safety Standards Series No. 85*, Vienna (2015).

[3] IAEA. (2017). Proceedings of the workshop on best practices in physics-based fault rupture models for seismic hazard assessment of nuclear installations (BestPSHANI). *International Atomic Energy Agency—IAEA*, Vienna 18–20 November 2015.

[4] Dalguer, L.A., Y. Fukushima, K. Irikura and Ch. Wu (2017). Best Practices in Physics-Based Fault Rupture Models for Seismic Hazard Assessment of Nuclear Installations: Introduction, Pure Appl. Geophys. 174 (2017), 3325–3329, DOI 10.1007/s00024-017-1673-0

[5] IAEA. (2019). Probabilistic Fault Displacement Hazard Analysis in Site Evaluation for Existing Nuclear Installations, *International Atomic Energy Agency— IAEA-TECDOC* (in preparation).

[6] Andrews, D.J (1976). Rupture velocity of plane-strain shear cracks, J. Geophys. Res., 81, 5679-5687.

[7] Day, S. M. (1982). Three-dimensional simulation of spontaneous rupture: the effect of nonuniform prestress, *Bull. Seismol. Soc. Am.,* 72, 1881-1902.

[8] Olsen, K. B., R. Madariaga, and R. Archuleta (1997). Three Dimensional Dynamic Simulation of the 1992 Landers Earthquake, *Science.* 278, 834-838.

[9] Dalguer, L.A., H. Miyake, S.M. Day and K. Irikura (2008), Surface Rupturing and Buried Dynamic Rupture Models Calibrated with Statistical Observations of Past Earthquakes. *Bull. Seismol. Soc. Am.* 98, 1147-1161, doi: 10.1785/0120070134.

[10] Galvez P, Dalguer LA, Ampuero JP, Giardini D (2016): Rupture reactivation during the 2011 Mw 9.0 Tohoku earthquake: Dynamic rupture and ground motion simulations, *Bull. Seismol. Soc. Am.,* Vol. 106, No. 3, pp. –, June 2016, doi: 10.1785/0120150153.

[11] Dalguer, L.A., H. Wu, Y. Matsumoto, K. Irikura, T. Takahama and M. Tonagi (2019**)**, Development of dynamic asperity models to predict surface fault displacement caused by earthquakes. *Pure Appl. Geophys (PAGEOPH).* DOI: 10.1007/s00024-019-02255-8.

[12] Irikura, K., and H. Miyake (2011). Recipe for predicting strong ground motion from crustal earthquake scenarios, *Pure Appl. Geophys.*, 168, 85-104, DOI:10.1007/s00024-010-0150-9.

[13] Irikura, K., S. Kurahashi and Y. Matsumoto (2019), Extension of characterized source model for long-period ground motion in near-fault area strong-motion-prediction recipe for near-source long-period. Pure Appl. Geophys. DOI: 10.1007/s00024-019-02283-4

[14] Shirahama, Y., M. Yoshimi, Y. Awata, T. Maruyama, T. Azuma, Y. Miyashita, H. Mori, K. Imanishi, N. Takeda, T. Ochi, M. Otsubo, D. Asahina and A. Miyakawa (2016), Characteristics of the surface ruptures associated with the 2016 Kumamoto earthquake sequence, central Kyushu, Japan, *Earth, Planets and Space* 68:191 DOI 10.1186/s40623-016-0559-1.

[15] Okada Y, Kasahara K, Hori S, Obara K, Sekiguchi S, Fujiwara H, Yamamoto A (2004) Recent progress of seismic observation networks in Japan Hi-net, F-net, K-NET and KiK-net. Earth Planets Space 56:xv–xxviii. doi:10.1186/BF03353076

[16] Aoi S, Kunugi T, Nakamura H, Fujiwara H (2011) Deployment of new strong motion seismographs of K-NET and KiK-net. In: Akkar S, Gülkan P, van Eck T (eds) Earthquake data in engineering seismology. Geotechnical, geological, and earthquake engineering, vol 14. Springer, Dordrecht, pp 167–186

[17] Nishimae Y (2004) Observation of seismic intensity and strong ground motion by Japan Meteorological Agency and local governments in Japan. J Jpn Assoc Earthq Eng 4(3):75–78

[18] Andrews, D. J. (1980), A stochastic fault model: 1. Static case, J. Geophys. Res.,85, 3867–3877.

[19] Ripperger, J., and P.M. Mai (2004). Fast computation of static stress changes on 2D faults from final slip distributions*, Geophys. Res. Lett.*, Vol. 31, No. 18, L18610 10.1029/2004GL020594.

[20] Asano and Iwata (2016), Source rupture processes of the foreshock and mainshock in the 2016 Kumamoto earthquake sequence estimated from the kinematic waveform inversion of strong motion data, Earth Planets Space, **68**:147, doi:10.1186/s40623-016-0519-9

